Advances in Science and Technology Research Journal

Advances in Science and Technology Research Journal, 2026, 20(4), 1–21
https://doi.org/10.12913/22998624/211735
ISSN 2299-8624, License CC-BY 4.0

Received: 2025.08.12
Accepted: 2026.02.15
Published: 2026.03.01

Thrust characteristics of the OSA-3 aircraft propulsion system with a two-stroke piston internal-combustion engine for selected propeller configurations.

Piotr Wróblewski[1,2*], Łukasz Kiszkowiak[2], Przemysław Bratkowski[1,2], Jarosław Milczarczyk[2]

[1] Faculty of Engineering, University of Technology and Economics H. Chodkowska in Warsaw, Jagiellońska 82f, 03-301 Warsaw, Poland
[2] Faculty of Mechatronics, Armament and Aerospace, Military University of Technology, ul. Gen. Sylwestra Kaliskiego 2, 00-908 Warsaw, Poland
* Corresponding author's e-mail: piotr.wroblewski@wat.edu.pl

ABSTRACT

This paper examines the thrust performance of a 3W-275Xi B2R TS CS two-stroke engine mounted on an OSA-3 aircraft, using different two- and three-blade propeller configurations. The tests were carried out on a test stand that enables the measurement of thrust force using a CL14 sensor and a CL450 recorder. The tests used propellers with different blade pitches, made of wood and carbon fiber. The results showed that the propeller's diameter has a higher influence on the generated thrust than the pitch itself. Increasing the propeller pitch was found to lead to higher thrust at high rotational speeds, but at the expense of higher engine load. The analysis showed that the selection of the propeller should always be individually adapted to the performance of the piston combustion engine and the intended application of the aircraft. An important functional criterion for the propulsion system is not only the maximum thrust, but also the torque performance of the engine. The novelty of this work lies in the design of a test stand that enables precise assessment of the influence of propeller geometry on thrust force. This allows us to explore new ways to improve the performance of propulsion systems in light and unmanned aircraft. The test results are highly significant in terms of selecting the appropriate propeller geometry for the aircraft's operational requirements. Another innovative feature of this paper is the development of a state-of-the-art test bench made up of an OSA 3 aircraft with cutting-edge engine performance measurement systems.

Keywords: experimental testing, two-stroke piston engine, aircraft propulsion thrust, propeller configuration, propulsion system optimization

INTRODUCTION

The rapid growth of light and unmanned aerial vehicles, combined with strict requirements for efficiency, reliability and control, poses a challenge for aerospace engineering. One important issue is improving the performance of two-stroke propulsion systems. Experimental tests are particularly important in this context. This enables the precise characterisation of the propulsion system's behaviour under various performance characteristics, as well as determining the influence of propeller geometry on the thrust generated by the piston combustion engine. In practice, choosing the right propeller for a specific engine and flight mission is crucial for optimising performance, economy and operational safety. With many propeller solutions on the market featuring different diameters, pitches and materials, design decisions must be supported by reliable experimental data. Acquiring them requires the application of advanced measurement methods.

Until recently, comprehensive thrust performance data for propulsion systems in light aviation, verified through direct measurements, have

been scarce. In recent years, modern test stands have been introduced that enable direct comparison of parameters such as thrust, energy consumption, and efficiency; however, the majority of these facilities focus on electric propulsion. Experimental research involving two-stroke piston internal combustion engines remains rare and is usually limited to laboratory or model-scale trials, leaving a significant gap in understanding their behavior under real operational conditions. These engines are highly sensitive to propeller geometry, particularly in terms of achievable thrust, which makes them challenging but valuable subjects of investigation.

The test bench presented in this paper addresses this gap by enabling detailed analysis of the dynamics and efficiency of conventional combustion propulsion systems in propeller configurations. The obtained results provide practical insights for the design and optimization of propulsion systems in both light and unmanned aviation, including military applications where reliability, durability, and proper engine–propeller matching to mission requirements are critical.

Small unmanned aerial vehicles (UAVs) are becoming increasingly popular among designers [3]. The most challenging aspect of the design process is selecting the right propulsion unit for the aircraft. Thorough analysis of the thrust force of the given propellers is required for such research. Although a fairly large number of studies have been conducted on thrust testing, these are limited and mainly concern propulsion units weighing more than 100 kg. As small aircraft are being used more frequently, it is essential that the propulsion unit and propeller profile are properly matched to the aircraft's intended use. Traditional performance evaluation methods require extensive wind tunnel testing [4].

Experimental propeller tests are also discussed at work [5]. The tests focused on developing a universal measurement system to accurately determine the performance of propellers implemented in UAVs, such as thrust, power consumption, and maximum revolutions per minute (RPM). The presented proprietary device can measure various types of BLDC motors and propellers and can test BLDC motors with a current consumption of up to 100 A [5]. The studies primarily involved testing electric motors, excluding combustion engines.

Paper [2] describes tests carried out on a device designed to measure the static thrust of light propeller aircraft. Measurements were taken on three aircraft with directly driven propellers of different diameters to test thrust in the range from idle to full throttle in various environmental conditions. The results showed that static thrust goes up with increasing propeller diameter and engine shaft speed. The static thrust estimation model was confirmed experimentally and the results obtained were consistent with theoretical predictions, particularly at low shaft speeds. The influence of temperature on thrust was also observed to be slight, and no influence of wind was observed up to a speed of 8.8 knots.

The following aircraft and engines are tested in the presented paper [2]:

- The Jabiru, powered by a four-stroke, four-cylinder, air-cooled engine with a capacity of 2200 cm^3. The propeller model used in the Jabiru (ZU-DAX) is the C000242-D60P42.
- The Cessna 150 (ZS-NAL), powered by a 100 hp (75 kW) Continental O-200-A engine. The propeller model used in the Cessna 150 (ZS-NAL) is a McCauley 1A102/OCM.
- The Cessna 172, equipped with a 150 hp (110 kW) Lycoming O-320-E2D engine. The propeller model used in the Cessna 172 (ZS-MWL) is a McCauley 1C160/CTM 7553.

Although the tests in paper [2] concern light aircraft and engines, the aircraft and engines used are in fact significantly heavier than the model tested. The aircraft used are quite large, and the engines have relatively high weight and geometric dimensions. In addition, the tests cover four-stroke engines. However, the paper does not attempt to explain how propeller geometry (e.g. blade angle of attack, number of propeller blades, and the application of different materials in their design) influence thrust and its performance.

Paper [6] presents the design of a test bench for measuring propeller parameters. This test bench is based on a simple frame and uses a strain gauge connected to the propulsion engine by a steel cable to measure thrust force. In this setup, Matlab-Simulink software was used to acquire the data, and an application generated a PWM signal for the ESC controller to control the engine [6]. Paper [7] presents a device based on a two-arm balancing mechanism designed to measure the thrust of propellers for micro-UAVs. Thrust was measured using a simple scale, independently of software. Another design for a test bench to measure propeller parameters is described in paper

[8]. These tests used a dynamometer designed for propellers with a diameter of up to 250 mm, which measures generated thrust and torque using strain gauge sensors.

Other methods of measuring propeller parameters are described in papers [9, 10], primarily for electric motors. However, these methods have not been verified using combustion engines, particularly light two-stroke engines. In paper [11], static thrust measurements were performed using strain gauge sensors and data acquisition systems. The thrust measurement results were then compared with those from an analytical method and computational fluid dynamics (CFD) simulations. The paper states that the analytical calculations differed from the experimental results by 5.08%, whereas the CFD calculations showed a deviation of 13.56%. These tests highlight the need for highly accurate measurements. It is difficult to take all the operating characteristics of two-stroke piston combustion engines into account in simulation studies, particularly those that may affect the thrust for a given propeller profile.

Papers [17,18] describe test benches and tests for small piston combustion engines designed for ultra-light aircraft. These papers also describe hybrid propulsion systems and the methodology for measuring engine performance on a test bench. Experimental studies to explain the aerodynamic processes of the propeller in both positive thrust and energy recovery modes were conducted in paper [12]. This paper indicates an option of recovering energy from the propeller using additional systems, which is very interesting. Such a solution could be applied to an auxiliary system for small piston combustion engines.

Until recently, comprehensive thrust performance data for propulsion systems in light aviation, verified through direct measurements, have been scarce. Modern test benches are now available, such as the Tyto Robotics Flight Stand 60, capable of measuring thrust up to 590 N, torque up to 30 N·m, shaft speed up to 280 s^{-1} (16,800 min^{-1}), fuel flow up to 13.3 mL/s, and temperature up to 1073 K, with sensors calibrated to ASTM standards [19]. This system provides high-precision data for engine–propeller matching and endurance testing [19]. However, most such facilities focus on electric or hybrid-electric propulsion. Studies on two-stroke piston engines are still uncommon, even though these engines offer a high power-to-weight ratio and are well suited for both light aircraft and UAVs. The test bench described in this paper helps fill this gap by allowing detailed measurements of combustion propulsion systems working with propellers.

Another example of a propulsion test stand is the WingFlying WF-CO-30 Coaxial Thrust Stand. It is built for testing two coaxial motors and propellers at the same time, but it can also test a single motor with a propeller. The stand measures thrust up to 294 N, torque up to 20 N·m, shaft speed in the range 0.5–250 s^{-1} (30–15,000 min^{-1}), current up to 150 A, and voltage up to 65 V. It uses optical sensors for rotational speed, infrared probes for temperature, and barometric sensors for pressure and humidity. The D-MET software shows all test data in real time and makes it possible to compare the performance of both rotors directly. These stands are mainly used for electric UAV propulsion tests, so applications with two-stroke piston engines are still very limited [20].

The WingFlying WF-EN-15 test bench is made for engines in the 35–110 cm^3 class. It can measure propeller thrust up to 490 N, torque up to 50 N·m, shaft speed up to 250 s^{-1} (15,000 min^{-1}), and works with propellers up to 1.27 m in diameter. The stand can test engines running on gasoline, methanol, or jet fuel. It uses optical and pulse sensors for rotational speed and has a torsion-bar system to reduce vibration, which makes it useful for both short laboratory runs and long endurance tests [21].

For larger engines, the WF-EN-50 extends the range to the 110–350 cm^3 class. It can measure thrust up to 1470 N, torque up to 150 N·m, and supports propellers up to 1.52 m. The stand includes software that records thrust, torque, efficiency, fuel use, and temperature in real time. Its modular layout allows it to be used not only for UAV engines but also for aerospace and automotive engine testing [22].In this work, an instrumented OSA-3-based test bench with continuous thrust acquisition was used. The stand enables continuous measurement of thrust force for multiple propeller variants. The novelty of the work is not only the construction of an advanced test stand, but also the determination of detailed thrust characteristics for different propellers under real operating conditions. Such data can be used for research on future numerical models. The obtained results allow appropriate matching of propeller geometric parameters to a specific engine and aviation tasks. Moreover, these studies make a significant contribution to the development of test methodology for propulsion systems used in unmanned and light aircraft.

Compared to the solutions described above, most available test stands are intended for electric propulsion or laboratory-scale experiments with combustion engines mounted on rigid frames. In contrast, the test bench presented in this paper employs a real OSA-3 airframe, which makes it possible to replicate operational conditions, but also introduces additional limitations related to the dynamics of the entire system (e.g., fuselage displacement during shaft speed transients). This approach provides unique experimental data that are difficult to obtain under purely laboratory conditions.In the context of the conducted tests with different propeller configurations, it is important to underline the significance of the engine–propeller matching process. As indicated in the literature [23], the proper matching of engine and propeller characteristics is a key factor in evaluating the performance of the entire propulsion system. A propeller should not be designed in isolation from engine parameters; otherwise, there is a risk of obtaining non-optimal thrust characteristics and excessive fuel consumption. The choice of propeller pitch and diameter directly defines the engine operating point, which affects take-off and climb performance as well as cruise efficiency in level flight.

This aspect is particularly important in modern electric and hybrid propulsion systems, where the engine efficiency map and the capability of the power supply system must be matched to the propeller power demand across the full operating envelope [24]. Research on tilt-propeller configurations has shown that proper matching of the propeller to the engine efficiency map not only improves propulsion efficiency but also reduces noise emissions by optimizing aerodynamic conditions and propulsion system loading.

The test bench presented in this study provides experimental data that support this process for two-stroke piston engines, where the sensitivity to propeller geometry is especially pronounced.

RESEARCH METHODOLOGY

Test bench design and key components

The test bench developed at the Aircraft Propulsion Research Laboratory uses the fuselage of an OSA 3 aircraft with a truss-type boom for mounting the tested engine (Figure 1 and Figure 2). Detailed information on the design of the OSA aircraft can be found in paper [13]. Thanks to its versatility, the OSA aircraft can be used by the military, the Border Guard, the Fire Brigade and other public safety institutions to observe and monitor potentially threatening situations [14]. The paper [15, 16] also present designs for the OSA aircraft's engine cooling and propulsion systems. These papers describe the requirements that must be met by selected propulsion systems to achieve the required flight performance.

A 3W-275Xi B2R TS CS engine has been mounted on the test bench. This two-cylinder piston combustion engine has a displacement of 273 cm³ and produces a maximum power output of 20.2 kW. The cylinder diameter is 59.00 mm, with a piston stroke of 50.00 mm. The engine speed range is between 1 000 and 7 000 min^{-1}. The engine's total weight, including the ignition system, is 7.030 g, and the shaft is designed with three ball bearings while the connecting rods have needle bearings at both ends. The tests used a fuel-oil mixture with an oil-to-petrol ratio of 1:40. The IIS ignition system is designed for a

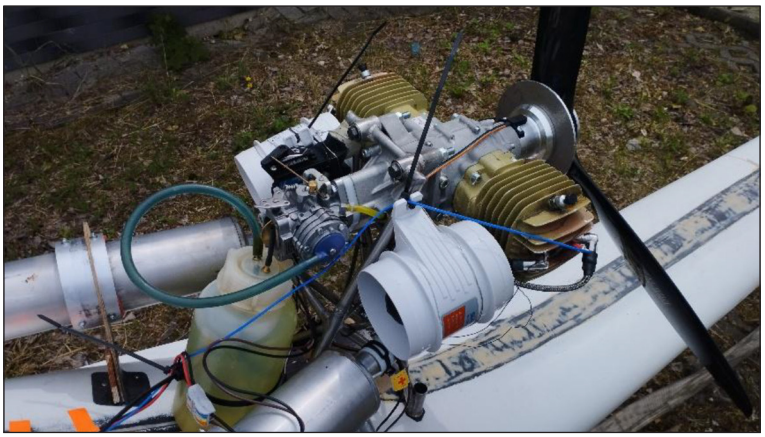

Figure 1. View of the mounted 3W-275Xi B2R TS CS engine on the OSA 3 aircraft

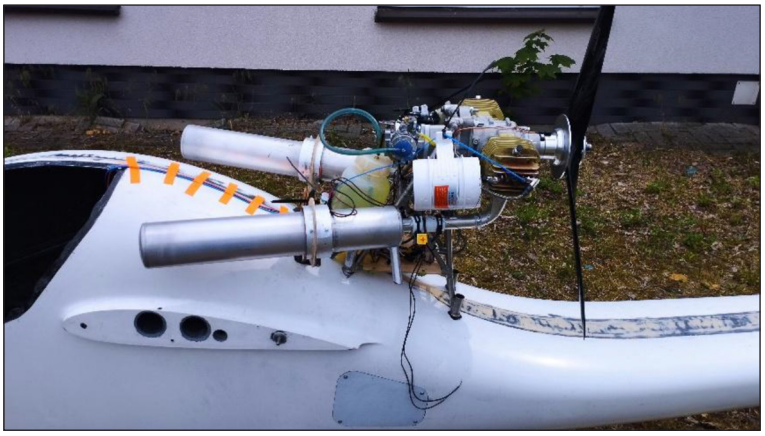

Figure 2. View of the 3W-275Xi B2R TS CS engine mounting frame from the side position of the engine on the OSA 3 aircraft

voltage range of 6.0–8.4 V. The entire assembly is mounted on a three-wheeled chassis. The test bench allows various types of propeller to be installed, including two- and three-bladed models with different blade profiles.

The test bench allows measurement of thrust, head temperature, vibrations, and noise. The most important components include SBS-01T telemetry temperature sensors, K FTARB04-K-M5P2 thermocouples and a Futaba FASS Test transmission system with T-FHSS Air technology. Thanks to these systems, the engine operation can be monitored continuously.

In the tests, a K FTARB04-K-M5P2 thermocouple, which is designed for mounting with an M5 screw, was used to measure the temperature of the heads in contact with the base material (Figure 3). The sensors have high accuracy (±0.75%t), which ensures reliable data in changing conditions.

The MAX6675 converter, used with K-type thermocouples, performs analogue-to-digital conversion of temperature signals over 0–1024 °C with 0.25 °C resolution. It includes a cold end compensation function and provides a 12-bit digital output in the serial peripheral interface (SPI) standard. Typical measurement error is up to 8 LSB in the 0–700 °C range. Low-noise amplifiers and built-in thermocouple circuit break detection are provided. The maximum SPI interface clock frequency is 4.3 MHz and the conversion time is approximately 220 ms.

The control components located in the OSA aircraft are shown in Figures 4 and 5.

Two SEAFLO SFIB2-235-04 fans provided auxiliary cooling airflow (400 $m^3 \cdot h^{-1}$ (235 CFM) with low current draw (max. 4 A). Units use a five-blade impeller with a sealed shaft and a corrosion-resistant ABS housing, are compatible with a 4″ / 102 mm inlet duct, and comply with

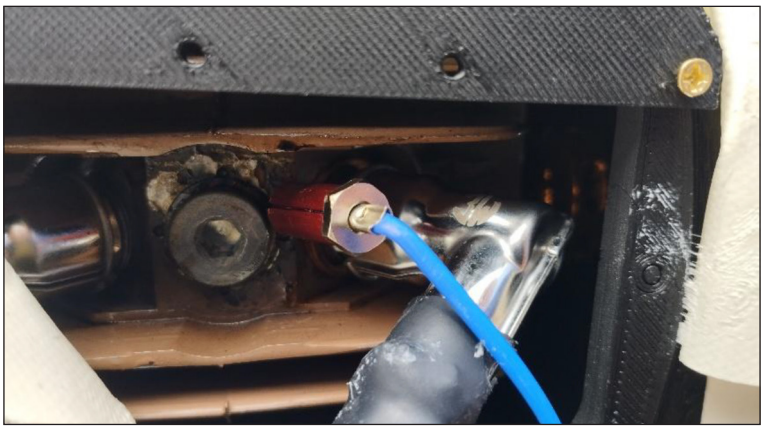

Figure 3. Method of mounting the FTARB04-K-M5P2 temperature sensor using fastening screws on the 3W-275Xi B2R TS CS engine

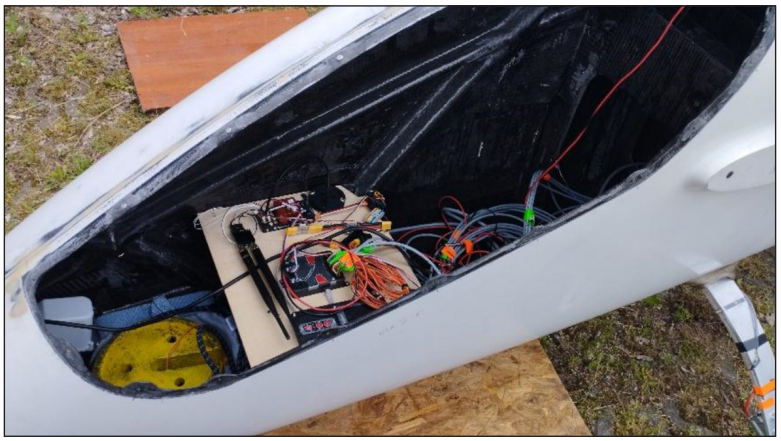

Figure 4. View of the mounted control components of the test stand

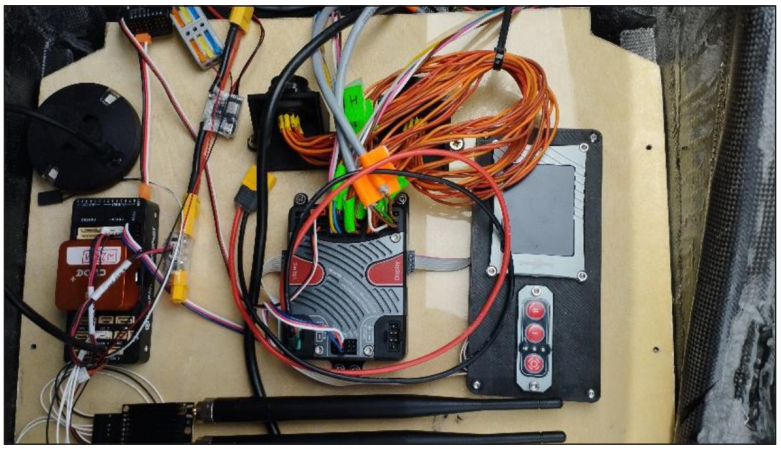

Figure 5. View of the control system assembly and transmitter

ISO 8846. A dedicated, quick-removal ventilation setup allowed on-stand installation/removal as required (Figure 6).

Static thrust was measured with a CL14 strain-gauge load cell (≤0.5% FS) aligned with the engine thrust line and interfaced to a CL450 single-channel data logger (thermal stability ≤0.05% per 10 K) (Figure 7). The load cell was attached via parallel straps to avoid off-axis components; no correction factors were required. Unless otherwise stated, the sampling rate was 1 Hz. This in-line instrumentation provided repeatable and directly comparable thrust measurements for all propeller configurations.

Figure 8 shows the position of force sensor suspended using special straps and connected to the ground via special connectors. This configuration of the measuring element enables the thrust force generated by the propulsion unit to be evaluated directly. Unlike test benches using a support frame [12], there is no need to apply correction factors in this case. The only condition is that the sensor straps must be positioned parallel to the engine's axis on the aircraft.

Calculating measurement error, uncertainty and the standard deviation of thrust force, taking into account all variables

Static thrust was measured using the in-line load-cell/data-logger chain described in Section 3.According to the manufacturer, the CL14 sensor has an accuracy of ≤0.5% of the measurement range. For the case under study, the calculations used a maximum thrust value of approximately 600 N.

Measurement error resulting from the CL14 force sensor (according to specifications: ≤0.5%)

$$\Delta_{sen} = 0.5\% \times 600\,\mathrm{N} = 0.005 \times \\ \times 600\,\mathrm{N} = 3\,\mathrm{N} \quad (1)$$

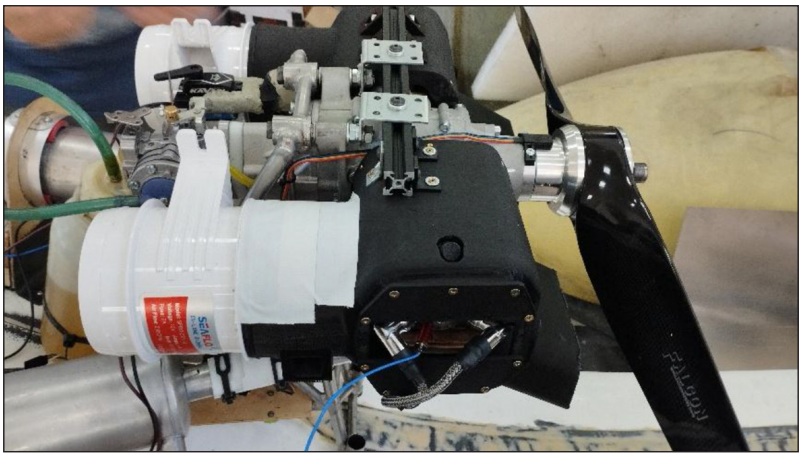

Figure 6. View of the SEAFLO SFIB2-235-04 fans with an additional airflow system

Figure 7. Mounting of the force sensor to the base frame of the OSA 3 aircraft assembly

The measurement uncertainty of the sensor CL14

The standard measurement uncertainty (specific to the strain gauge sensors) is usually taken as one-third of the error limit when assuming a rectangular distribution:

$$u_{sen} = \frac{\Delta_{sen}}{\sqrt{3}} = \frac{3}{1.732} \approx 1.73\ N \tag{2}$$

Impact of the CL450 data logger

Data-logger thermal drift was negligible relative to the dominant uncertainty sources.

The error resulted from the tension and the cable length (3 m)

Additional errors arise due to the cable's flexibility and deformation under load. The 3 m cable that transfers force from the aircraft model to the sensor can introduce two types of error:

- Error related to the elongation and elasticity of the cable (dynamic effect, vibration damping and micro-slips on the handles).
- Error resulting from the angle of inclination of the cable. This is also known as imperfect alignment with the measurement axis).

It was assumed that the cable was made of a high-strength material, such as Kevlar, and that it was minimally elastic; the error resulting from elongation could therefore be estimated according to Hooke's law. It was also assumed that this error would be approximately 0.3% of the measured force value, which is a typical figure for well-secured cables measuring 3 m in length.

$$\Delta_c = 0.3\ \% \times 600\ \text{N} = 0.003 \times 600\ \text{N} = 1.8\ \text{N} \tag{3}$$

$$u_c = \frac{\Delta_c}{\sqrt{3}} = \frac{1.8}{1.732} \approx 1.04\ N \tag{4}$$

Figure 8. View of the force sensor installation and layout of test components during thrust testing and noise level measurement

Total thrust measurement error

According to the principle of adding independent uncertainty errors (the square root of the sum of squares):

$$u_s = \sqrt{u_{sen}^2 + u_c^2} = \sqrt{(1.73)^2 + (1.04)^2} \approx \approx \sqrt{2.99 + 1.08} \approx 2.02\ N \quad (5)$$

Total boundary (maximum) measurement error

$$\Delta_s = \Delta_{\text{sen}} + \Delta_{\text{C}} = 4.8\ \text{N} \quad (6)$$

The thrust force was measured in the test bench using a CL14 force sensor with an accuracy of ≤0.5%. At a maximum thrust force of approximately 600 N, this corresponds to a measurement error of 3 N. Additional error was introduced by deformations and stresses in the 3-metre cable connecting the aircraft model to the sensor. This was estimated at 0.3% of the measured force, or approximately 1.8 N. Combining these uncertainties according to the principle of summing squares yielded a standard uncertainty in the measurement of approximately 2 N. Taking into account all variables, the maximum measurement error is 4.8 N, which is less than 1% of the bench's measurement range.

To calculate the measurement uncertainty of the propeller mass, data from the propeller's weight measurements (with values ranging from 273.0 g to 586.0 g) and the performance of the WLC 30/F1/K laboratory scale were employed. According to the manufacturer's documentation, the scale's resolution was d = 0.5 g and its measurement non-linearity was ±1.5 g.

Five measurements were taken for each propeller and identical weight readings were obtained each time, confirming the measurement's excellent repeatability.

Type A uncertainty (repeatability) was determined using the following formula:

$$u_a = \frac{s}{\sqrt{n}} \quad (7)$$

where: s is the standard deviation of the measurement series and n is the number of repetitions. As all the results were identical, the standard deviation was $s = 0$ and the type A u_a uncertainty was also 0.

Type B uncertainty, resulting from the performance of the device, consists of two main components. The first component is the uncertainty associated with the resolution of the scale display, which was calculated as follows:

$$\text{d} = 0.5\ \text{g} \rightarrow u_d = \frac{d}{2\sqrt{3}} = 0.144\ \text{g} \quad (8)$$

The second component is the uncertainty resulting from weight non-linearity:

$$\pm 1.5\ \text{g} \rightarrow u_{lin} = \frac{1{,}5}{\sqrt{3}} = 0.866\ \text{g} \quad (9)$$

The total standard measurement uncertainty was calculated by taking the square root of the sum of the squares of the two type B uncertainties.:

$$u_c = \sqrt{u_d^2 + u_{lin}^2} = = \sqrt{0.144^2 + 0.866^2} = 0.878\ \text{g} \quad (10)$$

The expanded uncertainty at a 95% confidence level (k = 2) was determined to be:

$$U = 2u_c = 1.756\ \text{g} \tag{11}$$

The results of the propeller weight measurements, together with the expanded and relative uncertainties, are presented in Table 1. The highest relative uncertainty did not exceed 1% (0.643% for the lightest propeller), which is fully acceptable in the context of propulsion system analysis. The obtained measurement uncertainty enables the propeller mass results to be used reliably in further strength and energy analyses. The maximum error of 4.8 N is less than 1% of the measurement range. This uncertainty does not affect the ranking of propellers, though it may be relevant when thrust differences are below 10 N.

TEST RESULTS AND DISCUSSION

Measurements of the thrust of the propulsion system

Thrust tests were performed twice for each propeller under the same external conditions of 25 °C and 30% humidity. Measurements were started after a 5-minute break had been taken and the input parameters had been reached. Initially, the temperature was approximately 50 °C for both sensors mounted on the outside of the engine heads. Thrust results depending on propeller speed were recorded continuously using a CL450 data logger. On average, one test trial comprises approximately 362 measurements until the maximum thrust and engine speed are reached. Figures 9–20 show that most measurements were recorded at high shaft speeds. This allows the maximum thrust values obtained to be determined more accurately. Similarly, it can be seen that the minimum engine shaft speed varies depending on the weight and load of the propeller used. Results from two tests allowed accurate determination of thrust depending on propeller type and profile. The parameters of the engine used and the weight of the propellers used for testing also play a significant role. These data are presented in Table 1. Throughout the entire paper, classical propeller designations in inches were used in accordance with the manufacturer's guidelines. In the table, an additional designation in SI units is provided. This facilitates navigation and referencing of individual models in this case, while remaining consistent with the manufacturer's labeling.

Figures 9 and 10 show the thrust performance of the Fiala 30 × 18 propeller. The maximum thrust, considering the aircraft's load and empty weight, is 403 N. The minimum engine speed is approximately 2 200 min^{-1}. In this case, the maximum engine speed was around 6450 min^{-1}. The results show that thrust begins to increase significantly above 3 200 min^{-1} and then rises almost linearly. Between 2 200 and 3 200 min^{-1}, thrust remains almost constant despite the increase in engine speed. Two measurement tests were conducted; the results were approximated using a power function.

Figures 11 and 12 illustrate the thrust performance of the Fiala 32 × 18 propeller. Although it has a higher diameter than the previous variant, it maintains the same pitch. Based on these figures, the minimum and maximum engine rotational speeds can be seen to be approximately 1 640 and 5 840 min^{-1}, respectively. The maximum thrust generated in both tests is approximately 422 N, increasing from a speed of around 2 200 min^{-1} – lower than for the Fiala 30 × 18 propeller. The thrust increase is approximately linear within the 3 500–5 840 min^{-1} range. The maximum thrust value was generated at an engine rotational speed that is 610 min^{-1} down compared to that of the previous variant.

The test results for the Fiala 32 × 16 propeller can be seen in Figures 13 and 14. In this case, the minimum engine rotational speed is

Table 1. Weight of propellers used in the tests [25]

Propeller name	Propeller weight [g]	Expanded uncertainty U (95%) [g]	Relative uncertainty U/m [%]
Fiala, 2-blade propeller 30 × 18 (762 × 457 mm)	273.0	1.756	0.643
Fiala, 2-blade propeller 32 × 16 (813 × 406 mm)	302.0	1.756	0.581
Fiala, 2-blade propeller 32 × 18 (813 × 457 mm)	299.5	1.756	0.586
Biela, 3-blade propeller 32 × 14 (813 × 356 mm)	586.0	1.756	0.300
Biela, 3-blade propeller 32 × 12 (813 × 305 mm)	547.5	1.756	0.321
Falcon, 3-blade propeller 32 × 13 (813 × 330 mm)	402.5	1.756	0.436

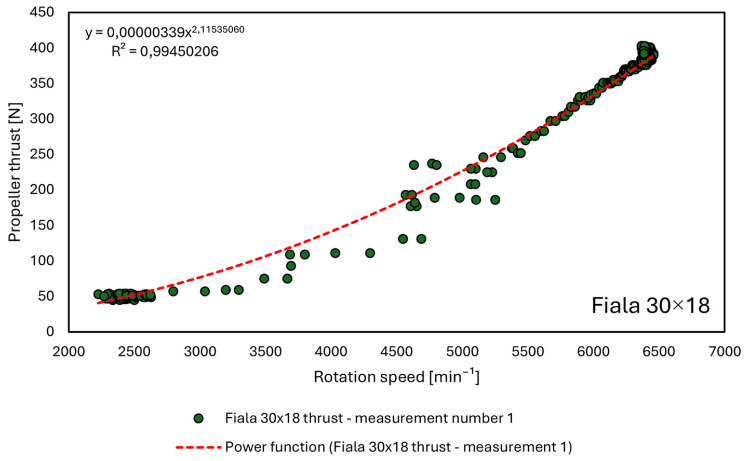

Figure 9. Thrust measurement for a 30 × 18 Fiala two-bladed wooden propeller – Test 1

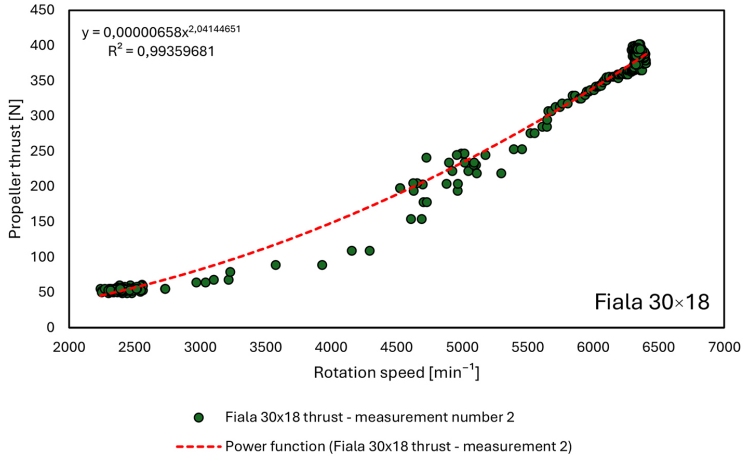

Figure 10. Thrust measurement for a 30 × 18 Fiala two-bladed wooden propeller – Test 2

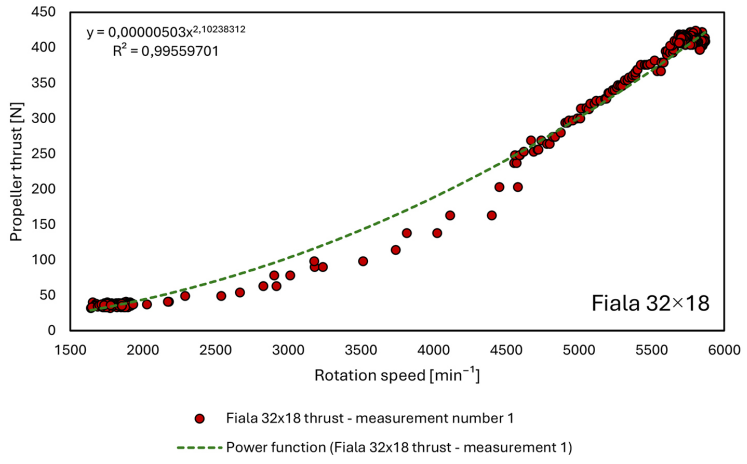

Figure 11. Thrust measurement for a Fiala 32 × 18 two-bladed wooden propeller – Test 1

approximately 1400 RPM, with a maximum value of around 6170 min^{-1}. Thrust increases linearly up to about 2500 min^{-1}. The maximum thrust value for the two test trials was 458 N, which is approximately 36 N up compared to that of the Fiala 32 × 18 propeller. However, this maximum thrust value is achieved at an engine rotational speed of approximately 330 min^{-1}, which is up compared to the previous propeller variant.

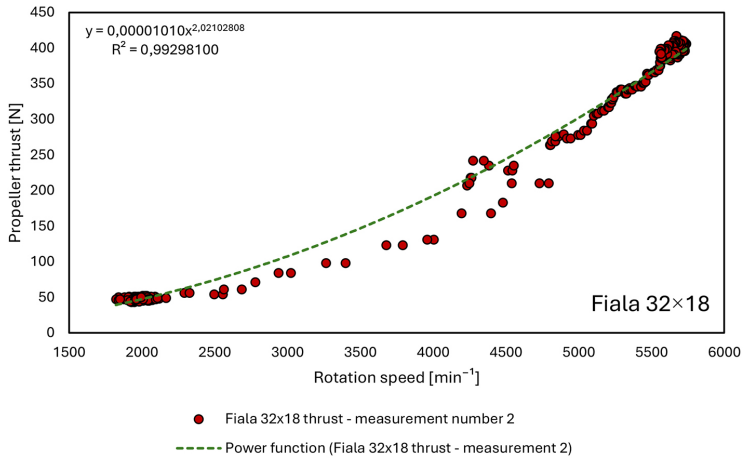

Figure 12. Thrust measurement for a Fiala 32 × 18 two-bladed wooden propeller – Test 2

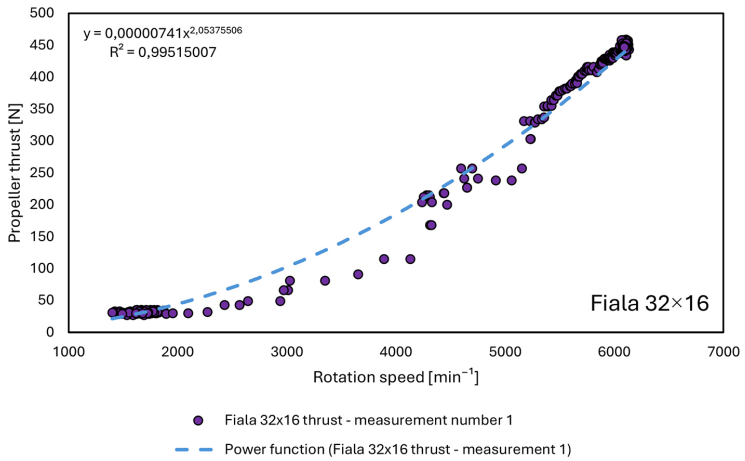

Figure 13. Thrust measurement for a Fiala 32 × 16 two-blade wooden propeller – Test 1

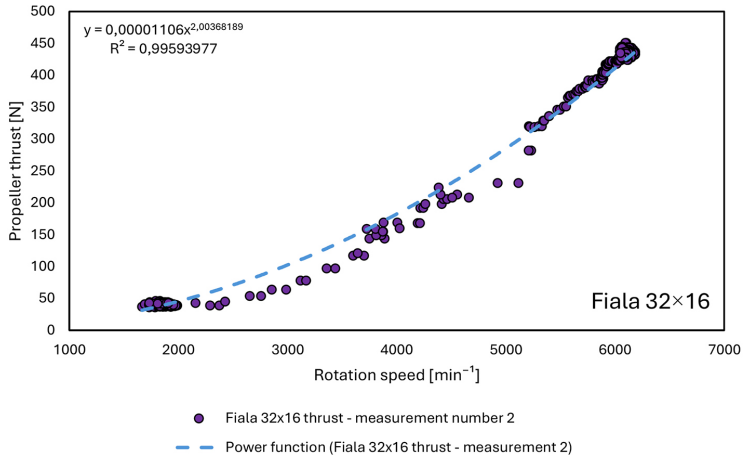

Figure 14. Thrust measurement for a Fiala 32 × 16 two-blade wooden propeller – Test 2

Figures 15 and 16 show the thrust curves for the Biela 32 × 12 propeller. The maximum thrust is approximately 489 N and the maximum engine shaft speed is around 5700 min^{-1}. While this propeller allows for a relatively low engine rotational speed of around 1000 min^{-1}, a significant increase in thrust is only achieved above 2000 min^{-1}. A substantial increase in thrust can

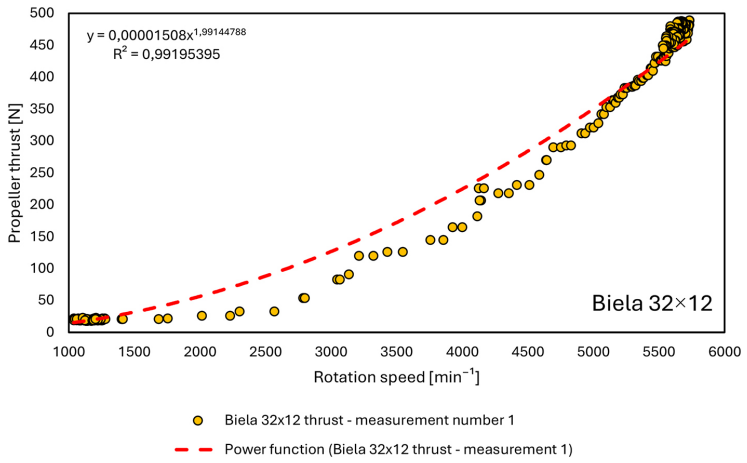

Figure 15. Thrust measurement for a Biela 32 × 12 three-blade carbon fibre propeller – Test 1

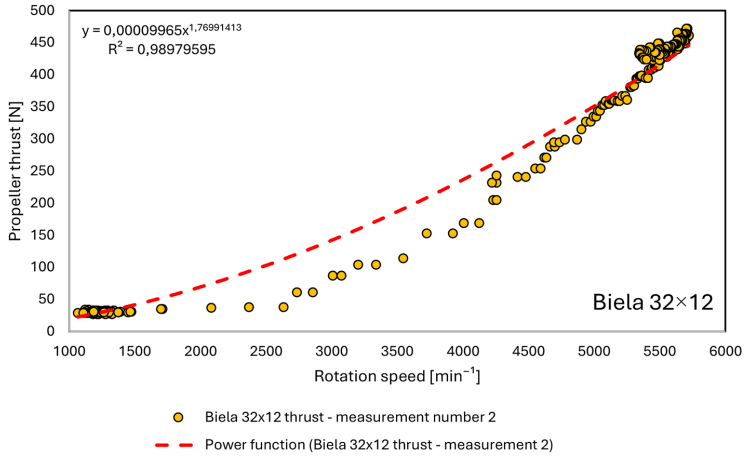

Figure 16. Thrust measurement for a Biela 32 × 12 three-blade carbon fibre propeller – Test 2

be achieved above 4500 min^{-1}. This propeller enables excellent performance in terms of thrust build-up speed.

As can be seen from Figures 17 and 18, which show the thrust performance for the Biela 32 × 14 propeller, this propeller generates a maximum thrust of approximately 427 N. The minimum engine speed is around 1000 min^{-1}, while the maximum is 4890 min^{-1}. This is significantly lower than the previous variant's engine speed. Changing the pitch from 12 to 14 reduced both the maximum engine speed and the maximum thrust. The maximum thrust was down by 62 N. In practice, a small propeller pitch enables high thrust at low engine rotational speeds and a high maximum shaft speed. Conversely, increasing the pitch enables a higher maximum engine rotational speed, but reduces thrust at low shaft speeds and increases the engine load. In this case, however, increasing the propeller pitch did not result in higher thrust or a higher maximum engine speed. The higher propeller pitch certainly increased the engine load to such an extent that it limited the maximum engine rotational speed. This confirms that each propeller and its profile must be selected individually for each engine.

Figures 19, 20 and 21 illustrate the thrust performance of the Falcon 32 × 13 propeller. As with the previous 3-blade propeller variants, the minimum engine speed is approximately 1000 min^{-1}. The maximum engine speed is around 5470 min^{-1}. The maximum thrust value is approximately 481 N, which is slightly down compared to that of the Biela 32 × 12 propeller. However, when the average values from two measurement tests are taken into account, the Falcon 32 × 13 propeller can boast of best performance among all 3-blade propellers.

Figure 22 illustrates the thrust performance of three variants of two-bladed wooden propellers,

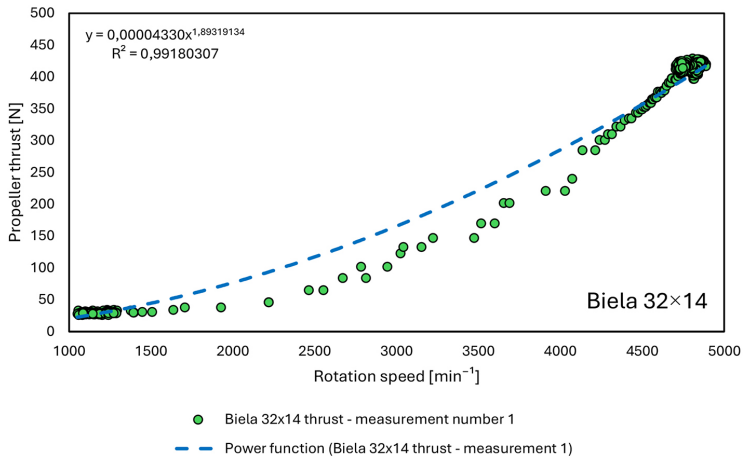

Figure 17. Thrust measurement for a 32×14 three-bladed carbon fibre propeller – Test 1

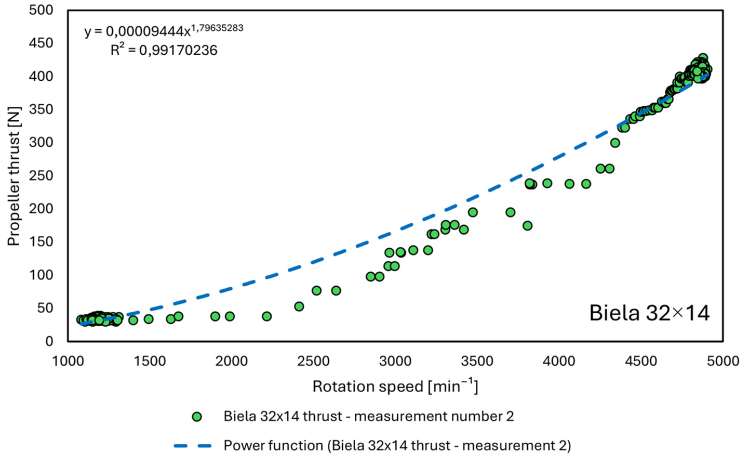

Figure 18. Thrust measurement for a 32×14 three-bladed carbon fibre propeller – Test 2

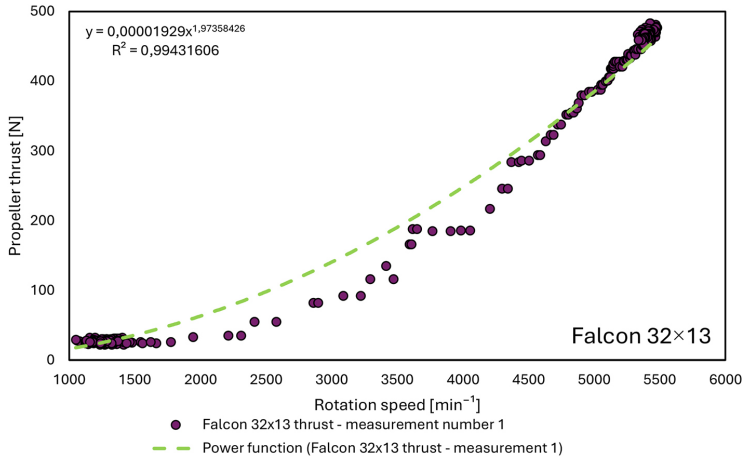

Figure 19. Thrust measurement for a three-blade, 32 × 13 carbon fibre Falcon 3 propeller – Test 1

which differ in terms of diameter and pitch. These performance were obtained by approximating two measurement trials for each propeller with a power function $T = \alpha n^b$. This provides significantly higher comparative reliability for all the propeller variants used. The thrust performance of three-bladed carbon fibre propellers were represented in the same way using a power

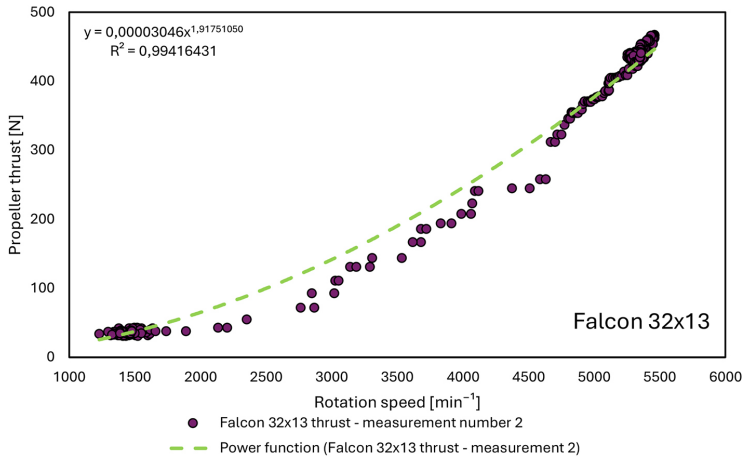

Figure 20. Thrust measurement for a three-blade, 32 × 13 carbon fibre Falcon 3 propeller – Test 2

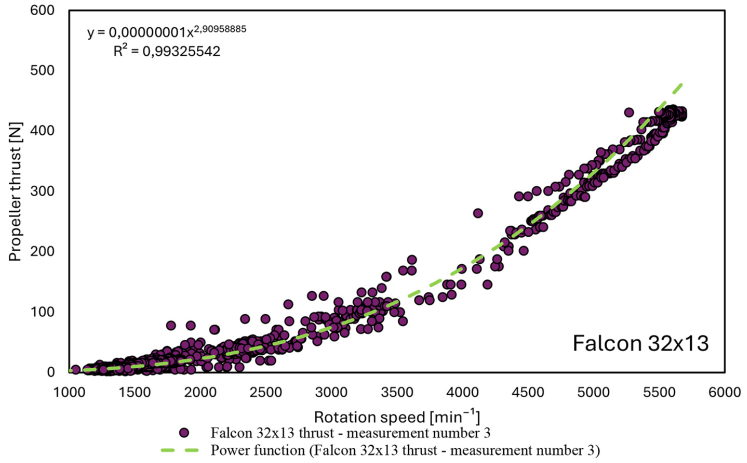

Figure 21. Thrust measurement for a three-bladed, 32 × 13, carbon fibre Falcon 3 propeller – Test 3 – sampling frequency: 10 Hz

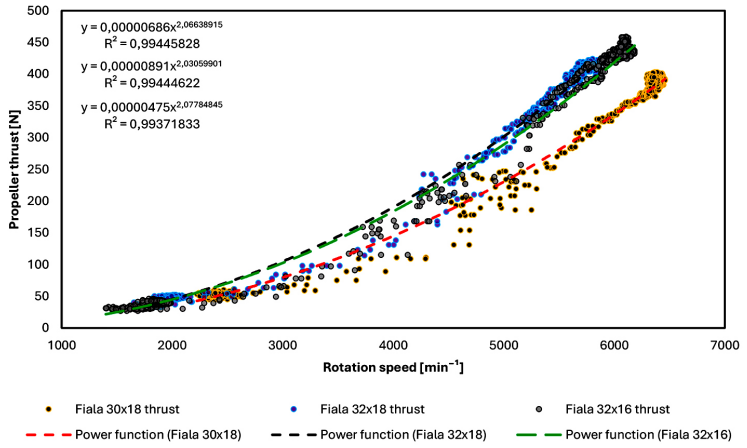

Figure 22. Thrust performance for 2-blade wooden propellers after approximation using a power function

function. According to Figure 15, the power-law exponents *b* range from 2.03 to 2.08, which is consistent with the theoretical Tan^2 scaling for fixed-pitch propellers [29, 30]. The propeller's diameter has a higher influence on thrust than its pitch. The 32-inch propellers (black and green performance) provide significantly more thrust than the 30-inch propeller (red performance)

across the entire shaft speed range. The +2″ diameter difference provides an additional thrust of approximately 60–70 N at 6000 min^{-1}.

The two 32-inch propellers, the Fiala 32 × 16 and the Fiala 32 × 18, differ in pitch by 2 inches. Up to a shaft speed of around 4000 min^{-1}, their thrust performance are almost identical. Above a shaft speed of ~4500 min^{-1}, however, the Fiala 32 × 18 propeller (black curve) provides an additional thrust of 10–15 N compared to the Fiala 32 × 16 propeller (green curve). These data were obtained by approximating the function from two measurements, so they may differ slightly from the comparative data for maximum thrust values in previous figures. Therefore, a larger propeller pitch allows for higher thrust at high shaft speeds, but at the cost of higher engine load. The very high coefficient of determination ($R^2 \approx 0.9958$–0.9972) indicates reliable measurement data and a correct model fit. The Fiala 32 × 18 propeller requires significantly more engine torque, so when selecting an engine for this configuration, the power reserve must be taken into account. Additionally, more noise can be expected at 6 000 min^{-1} due to the higher airflow velocity at the propeller blade tips.

The Biela 32 × 14 propeller generates the highest static thrust across the entire tested range of 1000 – 5700 min^{-1}. Its larger pitch increases thrust by an average of 20% compared to the Biela 32 × 12 and by 10–15% compared to the Falcon 32 × 13 at lower speeds of 4000 – 5000 min^{-1}. The engine must generate more torque in this case, and also run louder, because the higher pitch increases the airflow velocity at the blade tips. Although the Falcon 32 × 13 has a pitch that is 1 inch smaller, it has a steeper characteristic curve (power exponent ~1.55). Consequently, above approximately 5200 min^{-1}, it begins to generate higher thrust values and, at 5500 – 5700 min^{-1}, achieves even higher values than the Biela 32 × 14 propeller. This propeller reduces the load on the engine compared to the Biela 32 × 14. Therefore, a reasonable compromise is to use the Falcon 32 × 13 propeller with engines that achieve high maximum shaft speeds. This improves the efficiency of the propulsion unit. The 32 × 12 propeller generates the least thrust due to its small pitch. This propeller has two advantages: it significantly reduces the torque required from the engine (useful for units with limited power reserves) and it reduces noise because a smaller pitch means a lower blade tip speed at the same rotational speed.

The dependence of thrust on rotational speed for all three propellers is well described by the formula $T = \alpha \cdot n^b$, where b exponent is close to 1.5–1.55, while coefficient of determination $R^2 \approx 0.9937$–0.9944. This confirms the reliability of the measurements and allows the thrust to be extrapolated at any operating point. However, since thrust increases more slowly than the square of the speed, increasing the engine speed further above 5 800 min^{-1} is pointless due to the engine's limited performance and the increased airflow velocity at the blade tips. This results in enhanced noise emission. In practice, a 32 × 14 Biela propeller provides the best maximum thrust at moderate speeds (e.g. take-off, glider towing and heavy models), provided the engine can deliver a shaft speed of 4500 – 5000 min^{-1} without overheating or excessive fuel consumption. The Falcon 32 × 12 propeller offers excellent flexibility across the entire shaft rotational speed range, making it ideal for aerobatic flights. At high shaft speeds, the 32 × 13 Falcon propeller achieves a similar thrust to the 32 × 14 Biela propeller. However, this propeller offers the best response to an increase in shaft rotational speed (throttle opening), indicating a lower shaft load. The Biela 32 × 12 propeller is ideal for long flights or flights in areas with noise restrictions. It is an ideal solution for engines with lower torque.

The selection of a propeller should therefore be based not only on the maximum thrust obtained, but above all on the performance of the specific engine, taking into account the torque at given shaft speeds. Equally important are the aircraft's mission profile and noise limits for the area covered by the flight.

Figure 24 shows the relationship between the thrust generated by the Falcon 32 × 13 propeller and the engine shaft rotational speed at two sampling frequencies (1 Hz – green line; 10 Hz – red line). Both data series were approximated using a power function. For the 1 Hz measurements, a very high coefficient of determination was obtained ($R^2 = 0.9934$). For the 10 Hz sampling, $R^2 = 0.9932$ was achieved.

There is very good agreement between the approximation and the actual measurements for both data series ($R^2 > 0.99$), which confirms the reliability and repeatability of the tests. There is a clear, non-linear, increasing dependence of thrust on rotational speed: the higher the shaft rotational speed, the higher the increase in thrust. For measurements at lower frequencies (1 Hz),

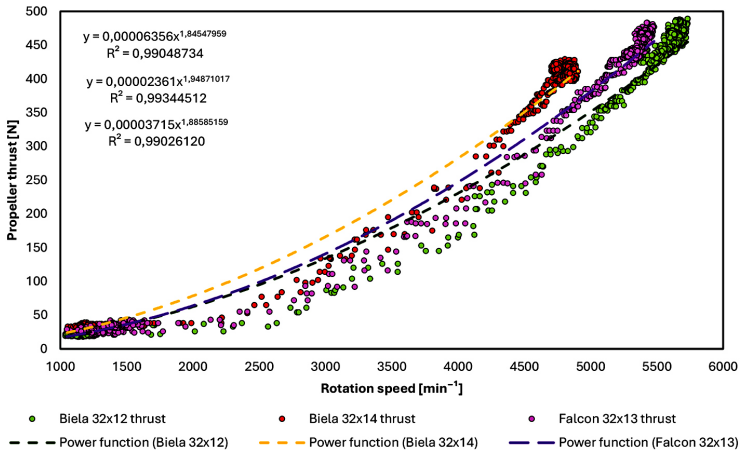

Figure 23. Thrust performance for 3-blade carbon fibre propellers, approximated using a power function

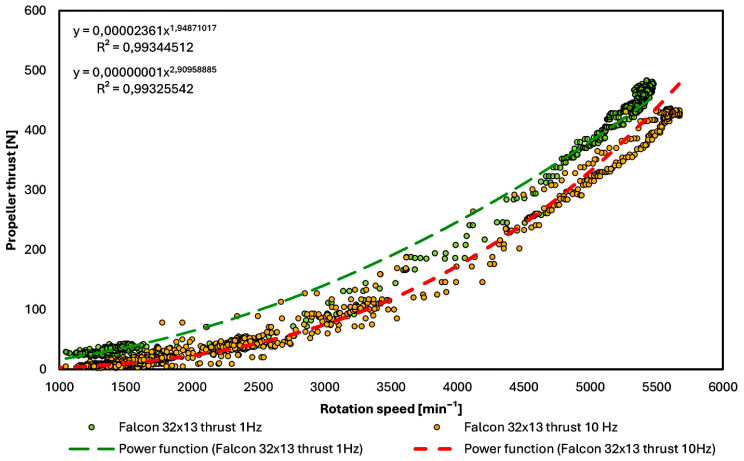

Figure 24. Comparison of thrust measurements for the Falcon 32 × 13 propeller at sampling frequencie of 1 and 10 Hz

the characteristic is smoother. At lower rotational speeds, thrust values are higher compared to measurements at 10 Hz. For higher shaft rotational speeds, however, the 10 Hz line shows a more rapid increase in thrust. This may indicate higher sensitivity and accuracy in detecting rapid changes at higher sampling rates, as well as the possible manifestation of dynamic propulsion system effects that are overlooked at lower sampling rates. Both models accurately reproduce the performance of the Falcon 32 × 13 propeller. This indicates that thrust depends strongly on shaft rotational speed and that the choice of sampling frequency affects how these relationships are recorded, which may be important for the precise analysis of propulsion performance in light and unmanned aviation.

Nevertheless, sampling at a frequency of 1 Hz is recommended for these measurements and the resulting differences. This is fundamentally justified in practice. Fast measurements involving rapid changes in shaft rotational speed cause errors to accumulate within the average speed range due to the sensor's response and that of its mounting system. In contrast, in measurements involving slow speed changes, the aircraft, which is connected to the sensor by a cable, smoothly changes its position, thereby altering the thrust. During rapid acceleration or deceleration of the shaft rotational speed, the aircraft temporarily moves backwards and exhibits uncontrolled movement. This was the main cause of the discrepancy in results obtained at 1 Hz and 10 Hz frequencies. In repeated tests involving a gradual increase in engine rotational speed, the results obtained at a sampling rate of 10 Hz were very similar to those obtained at 1 Hz. This proves that the sampling frequency merely increases the number of measurements in a series and does not significantly affect the

fundamental variation in measurement results. Therefore, it is reasonable to perform thrust measurements for this type of test bench at a frequency of 1 Hz.

Uncertainty quantification and impact on conclusions

Measurement uncertainty was evaluated for the complete thrust measurement chain and combined using standard methods. The resulting expanded uncertainty is small relative to the observed effects of propeller diameter and pitch. Inter-propeller differences in static thrust exceed this margin in all principal comparisons; therefore, the ranking of configurations remains unchanged. Where thrust deltas are comparable to the uncertainty, configurations are treated as operationally indistinguishable.

Data-acquisition rate was assessed for its influence on dispersion. Different sampling frequencies yield consistent results under steady conditions. During transients, increased scatter reflects test-stand dynamics rather than systematic bias. The nominal sampling frequency is therefore adequate for thrust mapping.

Study limitations

Measurements were conducted statically on a ground test stand. Actual operating conditions of the propulsion system for different aircraft flight configurations were not reproduced. The results in this work pertain to a single engine/airframe set (3W-275Xi B2R TS CS on OSA-3) and several propeller variants. Engine power and torque were not subject to experimental measurement. Engine loading was inferred on the basis of thrust–crankshaft rotational speed characteristics. Noise level, blade-tip Mach number, as well as aeroelastic effects and propeller–airframe interaction were outside the scope of the work. These investigations will be continued in future studies. The absence of these measurements does not affect the final conclusions.

STATISTICAL VERIFICATION AND SELECTION OF THE T(N) MODEL

Methodology

The relationship between thrust T and rotational speed nnn was modeled in two forms:

- *Power model:* $T = \alpha n^b$. Estimation was performed using ordinary least squares on the linearized data:

$$\ln T = \beta_0 + \beta_1 \ln n$$

where: $\beta_0 = \ln \alpha$, $\beta_1 = b$.

We report estimates $\hat{\beta}$, HC3 robust standard errors, t-statistics, p-values, and 95% confidence intervals.

- *6th-order polynomial model:* $T = \sum_k^6 \beta_k n^k$, fitted on the original T scale (OLS, HC3 errors).

Goodness-of-fit and model complexity were evaluated with adjusted R^2, AIC, and BIC [26,27]. The final model was selected based on AIC/BIC (lower is better) together with physical interpretability and extrapolation stability.

Editorial note (about R^2): the R^2 shown by Excel's "Power" trendline refers to fit on the original T scale, whereas the parameter estimation here is performed on the log–log scale. Therefore, the trendline R^2 may differ slightly from the adjusted R^2 reported for the log–log regression. In this thesis we consistently report: (1) α, b from log–log regression (HC3), (2) R^2 (log–log), and (3) AIC/BIC (for model selection).

Power model (physically motivated)

$$T = \alpha n^b \tag{12}$$

Linearization:

$$y = ln\, T,\ x = \ln n,\ y = \beta_0 + \beta_1 x + \varepsilon,\quad \beta_0 = ln\, \alpha,\ \beta_1 = b \tag{13}$$

Ordinary least squares (OLS) estimation:

$$\hat{\boldsymbol{\beta}} = (\mathbf{X}^\top \mathbf{X})^{-1} \mathbf{X}^\top \boldsymbol{y} \tag{14}$$

$$\mathbf{X} = \begin{bmatrix} \mathbf{1} & \boldsymbol{x_1} \\ \vdots & \vdots \\ \mathbf{1} & \boldsymbol{x_N} \end{bmatrix} \tag{15}$$

Residuals and variance:

$$\hat{\mathbf{u}} = \mathbf{y} - \mathbf{X}\hat{\boldsymbol{\beta}} \tag{16}$$

$$\boldsymbol{SSE} = \hat{\mathbf{u}}^\top \hat{\mathbf{u}} \tag{17}$$

$$\hat{\sigma}^2 = \frac{SSE}{N-p},\quad p = 2. \tag{18}$$

Covariance and robust standard errors (HC3) [28]:

$$\mathrm{Var}(\hat{\beta})_{\mathrm{HC3}} = (\mathbf{X}^\top \mathbf{X})^{-1} \mathbf{X}^\top \operatorname{diag}\left(\frac{\hat{u}_i^2}{(1-h_{ii})^2}\right) \mathbf{X} (\mathbf{X}^\top \mathbf{X})^{-1} \tag{19}$$

$$SE_{\mathrm{HC3}}(\hat{\beta}_j) = \sqrt{[\mathrm{Var}]_{jj}} \tag{20}$$

Significance testing and confidence intervals:

$$t(\hat{\beta}_j) = \frac{\hat{\beta}_j}{SE_{\mathrm{HC3}}(\hat{\beta}_j)} \tag{21}$$

$$CI_{95\%}(\hat{\beta}_j) = \hat{\beta}_j \pm t_{0.975,N-p} \cdot SE_{\mathrm{HC3}}(\hat{\beta}_j) \tag{22}$$

$$\hat{\alpha} = e^{\hat{\beta}_0} \tag{23}$$

$$CI_{95\%}(\alpha) = \left[e^{\hat{\beta}_0 - zSE}, e^{\hat{\beta}_0 + zSE}\right] \quad \text{for large } N\text{: } t \approx z \tag{24}$$

Goodness-of-fit measures (log–log scale) [26,27]:

$$\text{Adj. } R^2 = 1 - \frac{\frac{SEE}{N-p}}{\frac{SST}{N-1}}, \quad \mathrm{AIC} = N\ln\left(\frac{SEE}{N}\right) + 2p, \quad BIC = N\ln(SSE/N) + p\ln N \tag{25}$$

6th-order polynomial model

$$T(n) = \beta_0 + \beta_1 n + \beta_2 n^2 + \beta_3 n^3 + \beta_4 n^4 + \beta_5 n^5 + \beta_6 n^6 + \varepsilon \tag{26}$$

Estimation, t-tests, $\mathrm{Cl}_{95\%}$, Adj. R^2, AIC, BIC – as above, but on the T scale and with:

$$\mathbf{X} = \begin{bmatrix} 1 & n_1 & n_1^2 & \cdots & n_1^6 \\ \vdots & \vdots & \vdots & & \vdots \\ 1 & n_N & n_N^2 & \cdots & n_N^6 \end{bmatrix}, p = 7 \tag{27}$$

where: n – rotational speed [min^{-1}] (rpm), T – thrust [N]; $x = \ln n$, $y = \ln T$ – variables after linearization; $\beta_0 = \ln \alpha$, $\beta_1 = b$ – parameters in the log–log space.

Practical note: for n~10^3, the powers n^5, n^6 are on the order of 10^{15}–10^{18}, so the coefficients β_k are extremely small (e.g., -10^{18}). This is natural and can lead to poor numerical conditioning; for engineering use, the power model often behaves better.

Matrix notation

- $\mathbf{X}$ – design matrix (columns = functions of n or x).
- $\mathbf{y}$ – response vector.
- $\boldsymbol{\beta}$ – vector of coefficients.
- $\hat{\boldsymbol{\beta}}$ – OLS estimator vector.
- $\hat{\mathbf{u}} = \mathbf{y} - \mathbf{X}\hat{\boldsymbol{\beta}}$ – residual vector.
- $\mathbf{H} = \mathbf{X}(\mathbf{X}^\top\mathbf{X})^{-1}\mathbf{X}^\top$ – projection matrix;
- h_{ii} – leverage values.

Goodness-of-fit measures and tests

- $SSE = \sum_i \hat{u}_i^2$ – sum of squared errors.
- $SST = \sum_i (y_i - \bar{y})^2$ – total sum of squares.
- $R^2 = 1 - \frac{SSE/(N-p)}{SST/(N-1)}$ – adjusted R^2 (adjusts for the number of parameters p).
- AIC – Akaike information criterion: $\mathrm{AIC} = N\ln\left(\frac{SEE}{N}\right) + 2p$ (for ols with normal errors).
- BIC – Bayesian information criterion: $\mathrm{BIC} = N\ln\left(\frac{SEE}{N}\right) p\ln N$
- *HC3* – heteroskedasticity-consistent (robust) standard errors of White, HC3 variant (accounts for heteroskedasticity and leverage).
- $Cl_{95\%}$ – 95% confidence interval.
- *t-test* – significance test for an individual coefficient.

Example of calculations for the 30 × 18 Fiala two-bladed wooden propeller – Test 1

Power model

Estimates:

$\hat{\beta}_0 \approx -12.59368387$, $SE \approx 0.08530293$, $t \approx -147.6348$, $p < 0.001$
$\hat{\beta}_1 \approx \hat{b} \approx 2.1153505966965285$, $SE \approx 0.00974366$, $t \approx 217.1002$, $p < 0.001$

Confidence intervals:

$CI_{95\%}(\hat{\beta}_0) \approx [-12.761079 - 12.426289]$,
$CI_{95\%}(\hat{b}) \approx [2.0962533704105253, 2.1344478229825317]$

Back-transformed scale parameter:

$\hat{\alpha} \approx e^{\hat{\beta}_0} \approx 3.3933807129372313 \times 10^{-6}$
$CI_{95\%}(\alpha) = [2.8709299842828246, 4.0109068232156545] \times 10^{-6}$

Goodness-of-fit (log–log):

Adj. $R^2_{ln} \approx 0.99139536$, $AIC \approx -756.31150608$, $BIC \approx -748.53375017$.

Equation adopted for further analysis:

$$T(n) \approx 3.3933807129372313 \times$$

$$\times 10^{-6} n^{2.1153505966965285}$$

6th-order polynomial model (no reduction)

$$T(n) = 4.3075251596941 \times 10^{-12} +$$
$$+ 1.11676701557464 \times 10^{-8} n +$$
$$+ 1.05237008946423 \times 10^{-5} n^2 +$$
$$+ (-1.44322702855248 \times 10^{-9}) n^3 +$$
$$+ 2.02448107487722 \times 10^{-13} n^4 +$$
$$+ 4.83903691621185 \times 10^{-19} n^5 +$$
$$+ (-3.60419663930856 \times 10^{-21}) n^6$$

$\beta_0 \approx 4.30750 \times 10^{-12}$,
$\beta_1 \approx 1.11680 \times 10^{-8}$,
$\beta_2 \approx 1.05237 \times 10^{-5}$,
$\beta_3 \approx -1.44323 \times 10^{-9}$
$\beta_4 \approx 2.02448 \times 10^{-13}$,
$\beta_5 \approx 4.83904 \times 10^{-19}$,
$\beta_6 \approx -3.60420 \times 10^{-21}$ (HC3).

Goodness-of-fit (on T scale):

Adj. $R^2 \approx 0.99585987$, $AIC \approx 2669.18557315$, $BIC \approx 2688.62996295$.

Model choice: AIC/BIC clearly favor the power model

The equation adopted for further analyses and plots is:

$$T(n) \approx 3.3933807129372313 \times$$

$$\times 10^{-6} n^{2.1153505966965285}$$

DISCUSSION

The power model is compact, physically interpretable, and has substantially lower AIC/BIC than the 6th-order polynomial, even though the latter attains a very high R^2. High-order polynomials are often unstable outside the data range and can introduce artificial oscillations. Therefore, in the remainder of this work we use the power-law equation exclusively.

The report for the power model was conducted by classic log-log (OLS on ln T vs ln$n$) regression, and the result was given for Adj. R^2 on the log scale ($R^2_{ln} = 0.991395$). The software, when generating charts, shows R^2 calculated practically speaking on the original T scale for the curve $T = \hat{a} n^{\hat{b}}$ plotted on the chart (not on the log scale lnT). With that calculation, the value is 0.99450206. In this context, both approaches are correct for this type of power-law fitting.

CONCLUSIONS

The tests were performed in a specially built research stand using the 3W-275XI B2R TS CS engine mounted on the OSA-3 aircraft. The conducted tests allowed for a detailed analysis of the string for force characteristics for different types of propellers. Both two -boiled and three -go -fed -fiber fiber fiber propellers were tested. The research was conducted with various configurations of propellers with different diameters and jumps.

The most important conclusions from work include:

- The thrust performance is closely related to the propeller geometry and the engine's power and torque performance. Good performance of the propulsion system can only be achieved by selecting the propeller parameters (diameter, pitch, number of blades and material) individually to suit the aircraft's specific operational requirements.
- The experimental data and conclusions developed are particularly important for designers of light aircraft and military drones. This allows for the precise selection of propellers to meet operational requirements, resulting in increased propulsion efficiency, reduced fuel consumption, and improved engine safety and operational life. The data also provides a valuable basis for validating numerical models and developing CFD tools in aerospace engineering.
- The highest thrust is achieved by using propellers with a larger diameter. Propeller pitch only becomes crucial at higher shaft rotational speeds. A larger pitch allows for higher thrust, but requires significantly higher torque from the engine, increasing the load on the propulsion unit.
- The material used to manufacture the propeller significantly affects its performance. Carbon fibre propellers are more rigid and stronger, allowing for higher thrust values, and are therefore suitable for intensive work. Wooden propellers are lighter and more flexible, making them better suited to applications where low weight and smooth propulsion unit performance are a priority.

- The number of propeller blades has a significant impact on the level of thrust generated. Three-blade propellers generate higher thrust at lower rotational speeds than two-blade propellers, but they require higher torque from the engine and can put more load on the propulsion unit.

General practical conclusions:

- For long-endurance flights in areas with noise restrictions, propellers with a larger diameter and a smaller pitch are recommended, e.g. 3-blade Biela 32 × 12 made of carbon fiber. These propellers reduce the required torque, decrease noise, and support the reduction of fuel consumption. Further increasing the shaft rotational speed above approx. 5800 min^{-1} yields a diminishing increase in thrust force and an increase in noise perceived by the test stand operator. Therefore, it is not justified to use such high shaft rotational speeds.
- For aerobatic flights, propellers are recommended that provide a quick response to throttle opening changes and achieve high thrust values at high crankshaft rotational speeds, e.g. 3-blade Falcon 32 × 13. Above 5200 min^{-1} this propeller exceeds the thrust of the Biela 32 × 14 propeller.
- For flights with a high load – frequent take-off or transport of a large mass, e.g. a combat payload – 3-blade Biela 32 × 14 propellers are recommended. This propeller provides the highest thrust force at a relatively low shaft rotational speed (approx. 4500–5000 min^{-1}). If the engine has an adequate torque reserve and cooling system parameters. Alternatively, a Fiala 32 × 18 propeller (2-blade) can be used, which provides +10–15 N relative to 32 × 16 above ~4500 min^{-1}.

An OSA-3-based, in-line-instrumented test bench replicated the operational installation and eliminated correction factors, enabling precise, repeatable thrust characterisation and supporting model validation.

Acknowledgements

Research financed from the project: DOB-SZAFIR/01/B/038/04/2021 – funded by the National Centre for Research and Development, which was implemented in the Military University of Technology.

REFERENCES

1. Wróblewski P, Bratkowski P, Borcuch D, Kiszkowiak Ł. Prototype station dedicated to aircraft engine propeller profiles and advanced materials testing. Combustion Engines. 2025;201(2):165–175. https://doi.org/10.19206/CE-204319
2. Chen M. Static thrust measurement for propeller-driven light aircraft. In: Proceedings of the 2012 International Conference on Computer Application and System Modelling (ICCASM 2012); 2012;650–652. Paris: Atlantis Press. https://doi.org/10.2991/iccasm.2012.165
3. Gundlach J. Designing unmanned aircraft systems: a comprehensive approach. Reston (VA): American Institute of Aeronautics and Astronautics; 2012.
4. Kimberlin RD. Flight testing of fixed-wing aircraft. Reston (VA): American Institute of Aeronautics and Astronautics; 2003.
5. Kósa P, Kišev M, Vacho L, Tóth L, Olejár M, Harničárová M, Valíček J, Tozan H. Experimental measurement of a UAV propeller's thrust. Tehnički vjesnik. 2022;29(1):73–80. https://doi.org/10.17559/TV-20201212185220
6. Jakubowski A, Kubacki A, Minorowicz B, Nowak A. Analysis thrust for different kind of propellers. In: Advances in Intelligent Systems and Computing. Progress in Automation, Robotics and Measuring Techniques. Cham: Springer; 2015;85–90. https://doi.org/10.1007/978-3-319-15796-2_9
7. Zabunov S, Mardirossian G. Scales for measuring UAV micro-motor static thrust. Aerospace Research in Bulgaria. 2018;30:96–102. https://doi.org/10.3897/arb.v30.e08
8. Hossain MR, Krouglicof N. Propeller dynamometer for small unmanned aerial vehicle. In: 2010 Canadian Conference on Electrical and Computer Engineering (CCECE); 2010;1–5. https://doi.org/10.1109/ccece.2010.5575152
9. Kotarski D, Krznar M, Piljek P, Simunic N. Experimental identification and characterization of multirotor UAV propulsion. J Phys Conf Ser. 2017;870:012003. https://doi.org/10.1088/1742-6596/870/1/012003
10. Szafranski G, Czyba R, Blachuta M. Modelling and identification of electric propulsion system for multirotor unmanned aerial vehicle design. In: 2014 International Conference on Unmanned Aircraft Systems (ICUAS); 2014;1–8. https://doi.org/10.1109/icuas.2014.6842287
11. Khasyofi M, Hartono F. Development testing method and analysis static thrust for propeller-based propulsion. IOP Conf Ser Mater Sci Eng. 2019;645:012015. https://doi.org/10.1088/1757-899X/645/1/012015
12. Nederlof R, Ragni D, Sinnige T. Energy-harvesting performance of an aircraft propeller. J Aircraft. 2025;62(2):349–369. https://doi.org/10.2514/1.C038005

13. Olejnik A, Dziubiński A, Kiszkowiak Ł. Reliable method of aerodynamic analysis using computational fluid dynamics and scaled models in the development process of a Very Light Airplane. IOP Conf Ser Mater Sci Eng. 2021;1024:012048. https://doi.org/10.1088/1757-899X/1024/1/012048
14. Olejnik A, Kiszkowiak Ł, Rogólski R, Chmaj G, Radomski M, Majcher M, Omen Ł. The use of unmanned aerial vehicles in remote sensing systems. Sensors. 2020; 20: 2003. https://doi.org/10.3390/s20072003
15. Olejnik A, Kiszkowiak Ł, Dziubiński A, Majcher M. Cooling improvement of an aircraft engine in pusher configuration. In: 2021 IEEE 8th International Workshop on Metrology for AeroSpace (MetroAeroSpace); 2021 Jun 23–25; Naples, Italy. New York: IEEE; 2021;58–62. https://doi.org/10.1109/MetroAeroSpace51421.2021.9511781
16. Olejnik A, Kiszkowiak Ł, Dziubiński A. Ventilation analysis of simplified engine nacelle for pusher aircraft. IOP Conf Ser Mater Sci Eng. 2022; 1226(1): 012037. https://doi.org/10.1088/1757-899X/1226/1/012037
17. Wróblewski P, Świątek P, Kachel S, Zyska T. Development and research of a hybrid power unit for ultralight aircraft: an innovative approach to energy efficiency and operational flexibility. Combustion Engines. 2024;197(2):83–96. https://doi.org/10.19206/CE-174721
18. Wróblewski P. Analysis of torque waveforms in two-cylinder engines for ultralight aircraft propulsion operating on 0W-8 and 0W-16 oils at high thermal loads using the diamond-like carbon composite coating. SAE Int J Engines. 2022;15(1). https://doi.org/10.4271/03-15-01-0005
19. Tyto Robotics. New flight test stand for UAV engines & propellers. Unmanned Systems Technology. 2025 Jan. https://www.unmannedsystemstechnology.com/2025/01/new-flight-test-stand-for-uav-engines-propellers
20. WingFlying. WF-CO-30 coaxial thrust stand drone test bench. 2024. Available from: https://beyondsky.xyz/wf-co-30kgf-coaxial-thrust-stand-228
21. WingFlying. WF-EN-15 engine test bench. Wing Flying Technologies Co., Ltd.; 2024a. Available from: https://wing-flying.com
22. WingFlying. WF-EN-50 engine test bench. Wing Flying Technologies Co., Ltd.; 2024b. Available from: https://wing-flying.com
23. Gur O, Feldman J. Engine–propeller matching. In: Proceedings of the 62nd Israel Annual Conference on Aerospace Sciences (IACAS); 2023; Tel Aviv, Israel.
24. Bergmann O, Möhren F, Frey D, Braun C. Evaluation of aeroacoustic optimisation strategies for a generic flight mission of a tilt-propeller aircraft. Energies. 2025; 18(2). https://doi.org/10.3390/en18020345
25. Wróblewski P, Bratkowski P, Kachel S. Investigation of the influence of propeller blade profile and angle of attack on the performance parameters of an aircraft piston engine. Combustion Engines. https://doi.org/10.19206/CE-208772
26. Akaike H. A new look at the statistical model identification. IEEE Trans Autom Control. 1974;19(6):716–723. https://doi.org/10.1109/TAC.1974.1100705.
27. Schwarz G. Estimating the dimension of a model. Ann Stat. 1978; 6(2): 461–464. https://doi.org/10.1214/aos/1176344136.
28. MacKinnon JG, White H. Some heteroskedasticity-consistent covariance matrix estimators with improved finite sample properties. J Econom. 1985; 29(3): 305–325. https://doi.org/10.1016/0304-4076(85)90158-7.
29. McCormick BW. Aerodynamics, Aeronautics and Flight Mechanics. 2nd ed. New York: Wiley; 1995.
30. Leishman JG. Principles of Helicopter Aerodynamics. 2nd ed. Cambridge: Cambridge University Press; 2006.